Polymers & biopolymers

Helical core-sheath elastic yarn-based dual strain/humidity sensors with MXene sensing layer

Lihong Wang[1,2,3], Mingwei Tian[1,2,3,*], Yuying Zhang[1,2,3], Fengqiang Sun[1,2,3], Xiangjun Qi[1,2,3], Yiming Liu[4], and Lijun Qu[1,2,3,*]

[1] College of Textiles and Clothing, Qingdao University, Qingdao 266071, People's Republic of China

[2] State Key Laboratory of Bio-Fibers and Eco-Textiles, Qingdao University, Qingdao 266071, People's Republic of China

[3] Collaborative Innovation Center for Eco-Textiles of Shandong Province, Qingdao University, Qingdao 266071, People's Republic of China

[4] School of Control Science and Engineering, Shandong University, Jinan 250061, People's Republic of China

ABSTRACT

Flexible, stretchable and sensitive textile-based sensors play important roles in a wide variety of artificial intelligence because of its seamless integration with clothing and good comfort. Herein, MXene sensing layer is deposited on the surface of springlike helical core-sheath polyester yarns thanks to the capillarity effect and its intrinsic hydrophilic ability, and the resultant strain sensor and humidity sensor exhibit wide detection range from 0.3 to 120% strain and 30–100% relative humidity (RH) detection, owing to elastic core-sheath structures. The strain sensor shows excellent reproducibility (over 10000 cycles) and fast response time (120 ms). The core-sheath yarn sensor can detect various human motions such as walking, bending and twisting as well as physiological signal (pulse), which have great potential in real-time precise medicine and health care. The yarn sensor could also be an excellent humidity sensor because of the high specific area structure of yarn and intrinsic hydrophilic properties of MXene sensing layer.

Introduction

Flexible electronics is an important part of next-generation wearable devices, such as flexible microcontrollers, flexible sensors and flexible actuators [1–5]. Textile-based sensors seamlessly assembled from flexible sensors have not only wider myriad applications, such as personalized health-monitoring, human motion detection, human–machine interfaces and soft robotics, but also are more comfortable and convenient. Therefore, various flexible wearable strain sensors have been developed, such as elastomer, hydrogel and fabrics are used as the substrates to increase the flexibility and tensile properties of strain sensors [6–9]. And conductive materials such as graphene [10], carbon nanotubes [11] and some metal materials [12] are often combined with flexible substrates to assemble sensors. However, the

conductive materials have insufficient bonding force and require the bonding of other adhesives to bond with flexible substrates [10, 12]. As an emerging two-dimensional conductive material, MXene has excellent electrical conductivity and functional groups that can be stable connected to fiber substrate [13, 14]. Therefore, textile-based sensors which combine MXene with textile substrates have higher sensitivity and durability as strain sensors [6, 13, 15] and humidity sensors [16, 17]

Herein, a springlike core-sheath yarn is proposed with textile substrates and MXene combined as a textile-based strain sensor and humidity sensor. Such sensors exhibit not only sensing performance but also seamlessly connection with clothes due to the intrinsic sensing performance of the conductive core-sheath yarn. As a proof of concept, we also employed the strain sensors to monitor diversified sensing responses from human motions and subtle physiological signals.

Experimental

Core-sheath yarn (CSY) was spun in our laboratory with a spinning trial machine (DSSp-02B, Jiacheng, Tianjin), one polyurethane filament (PU) (fineness 75D) was five-fold pre-drawn with the tensioner and the yarn guide and then fed polyester filament (PET) (fineness 100D) into a set of rollers simultaneously, the two mixed groups of filaments were twisted together to form the core-sheath yarn, and after releasing the loading pre-drawn, the PU filament retracted to the original length leading to the helical PET sheath filaments around the PU core filament.

The CSYs were first cleaned ultrasonically in water for 30 min to remove the additional wax and impurity. After drying, the CSYs fixed on a tube were immersed into the inks for 10 min, and due to the capillarity effect of the fibrous structure, the inks were absorbed immediately, and the "wet" yarns were then placed in the oven for 10 min drying at 120 °C to remove the water. The helical conductive CSYs were finally obtained.

The gauge factor (GF) of the sensors can be calculated from equation as follows:

$$GF = \left(\frac{|R - R_0|}{R_0}\right) \bigg/ \left(\frac{\Delta L}{L_0}\right) \qquad (1)$$

where R and R_0 are the real time and original resistance of the sensors, respectively, and $\Delta L/L_0$ is the strain rate.

The sensitivity (S), which is a representative parameter employed to characterize the humidity-sensing property, was calculated using the following equation:

$$S = \frac{\Delta R}{\Delta RH} \qquad (2)$$

where ΔR is the resistance change over the whole detection range (30–99% RH) and ΔRH is the value of ambient RH change from the lowest to the highest (99–30% RH).

Results and discussion

The structure of the core-sheath yarn and the capillary effect

Figure 1 illustrates the fabrication of the flexible MXene-based core-sheath yarn strain sensor. The spinning technology of CSY was employed PU as core and PET as sheath (Fig. 1a). After dip coating in MXene inks (5 mg/mL), the color of CSY varied from white to black, and then MXene-based core-sheath yarn (MCSY) strain sensor was obtained after drying in oven (Fig. 1b). The capillary effect of yarn is verified in Fig. 1c; MXene inks can gradually climb along with yarns 0.9 mm within 10 s.

Chemical characterization and sensing principle of MCSY

The "compression spring" structure resulted by the helical structure of PET filaments winding around the PU core filament can be clearly observed for the pristine core-sheath yarns (Fig. 2a). After dip coating in MXene inks, the surface of individual PET filament is uniformly covered with MXene nanosheets (Fig. 2b), and the elemental mapping by energy-dispersive X-ray spectroscopy (EDS) was assigned to the distribution of C, O, F and Ti elements on the fiber surface. For the FTIR spectrum (Fig. 2c), compared with CSY spectrum, some stretching vibrations of –OH at 3430 cm^{-1}, C=O at 1712 cm^{-1} and O–H at around 1390 cm^{-1} were obviously enlarged, and the typical peak at 665 cm^{-1} and 1100 cm^{-1} of Ti–O and C–F appears owing to the incorporation of MXene
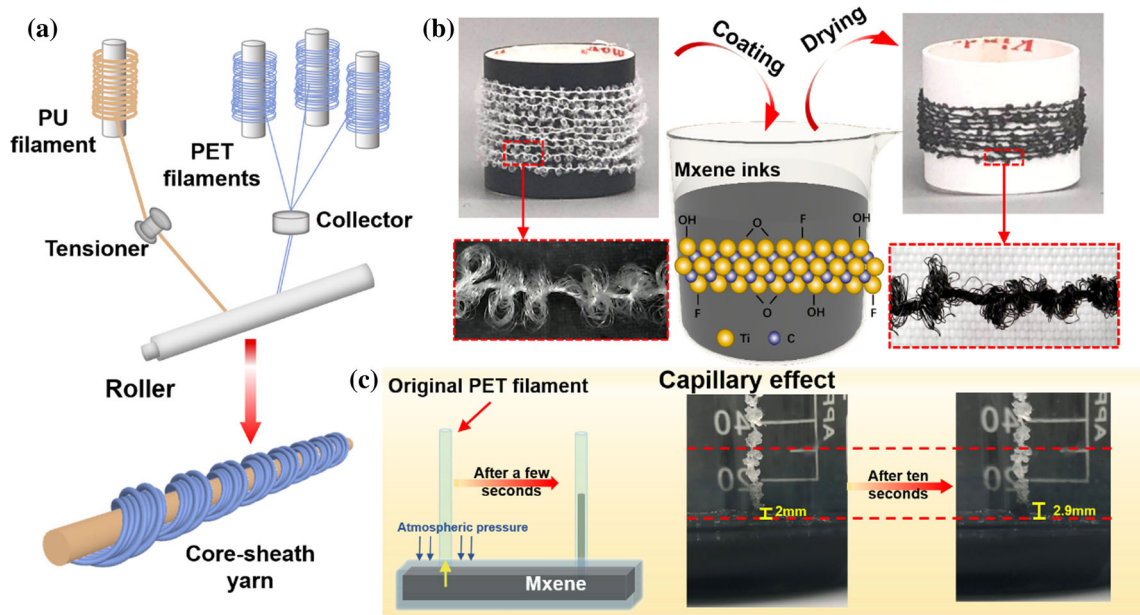
Figure 1 **a** The spinning route of core-sheath yarns. **b** Fabrication process of MXene-based core-sheath yarns. **c** The phenomenon of capillary effect.
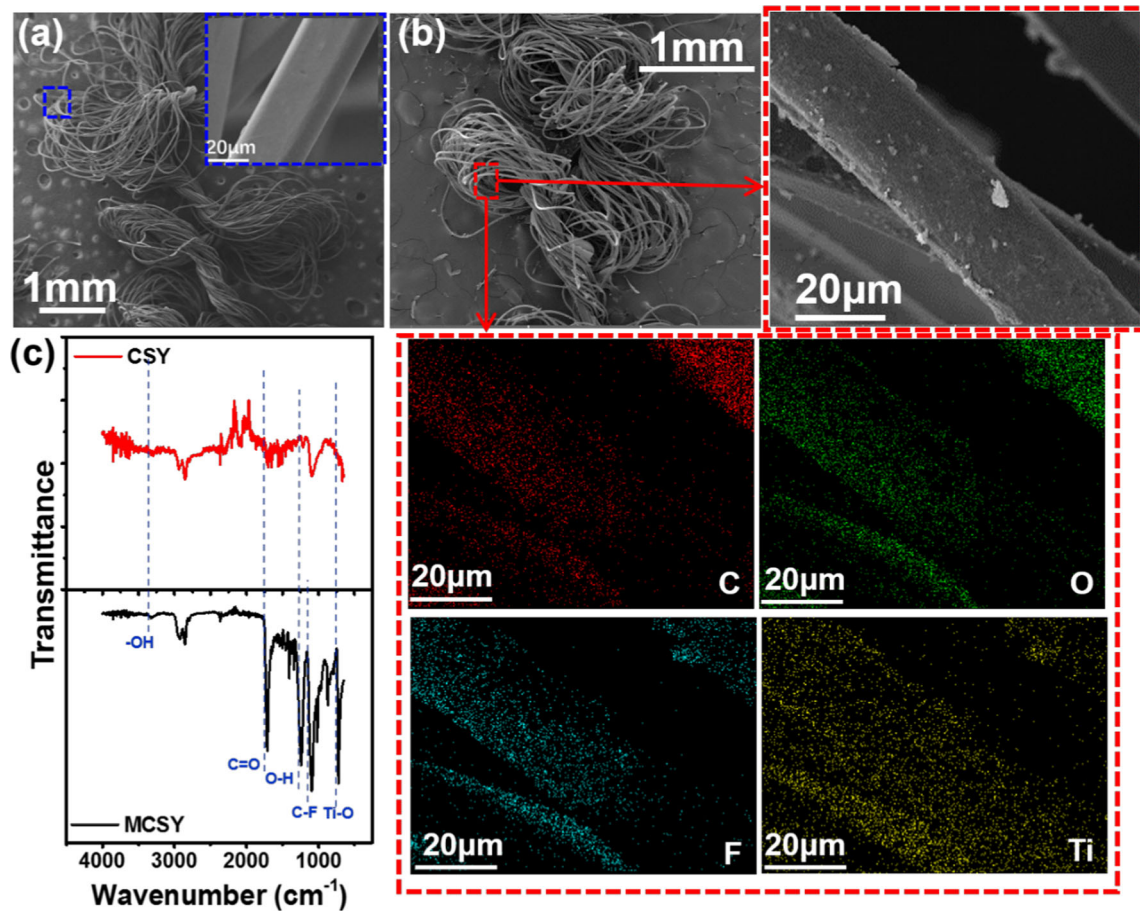

Figure 2 **a** SEM images of CSY and the surface of PET filament. **b** SEM images of MCSY, the SEM images and elemental mapping images of PET filament from MCSY. **c** FTIR spectra of the CSY and MCSY.
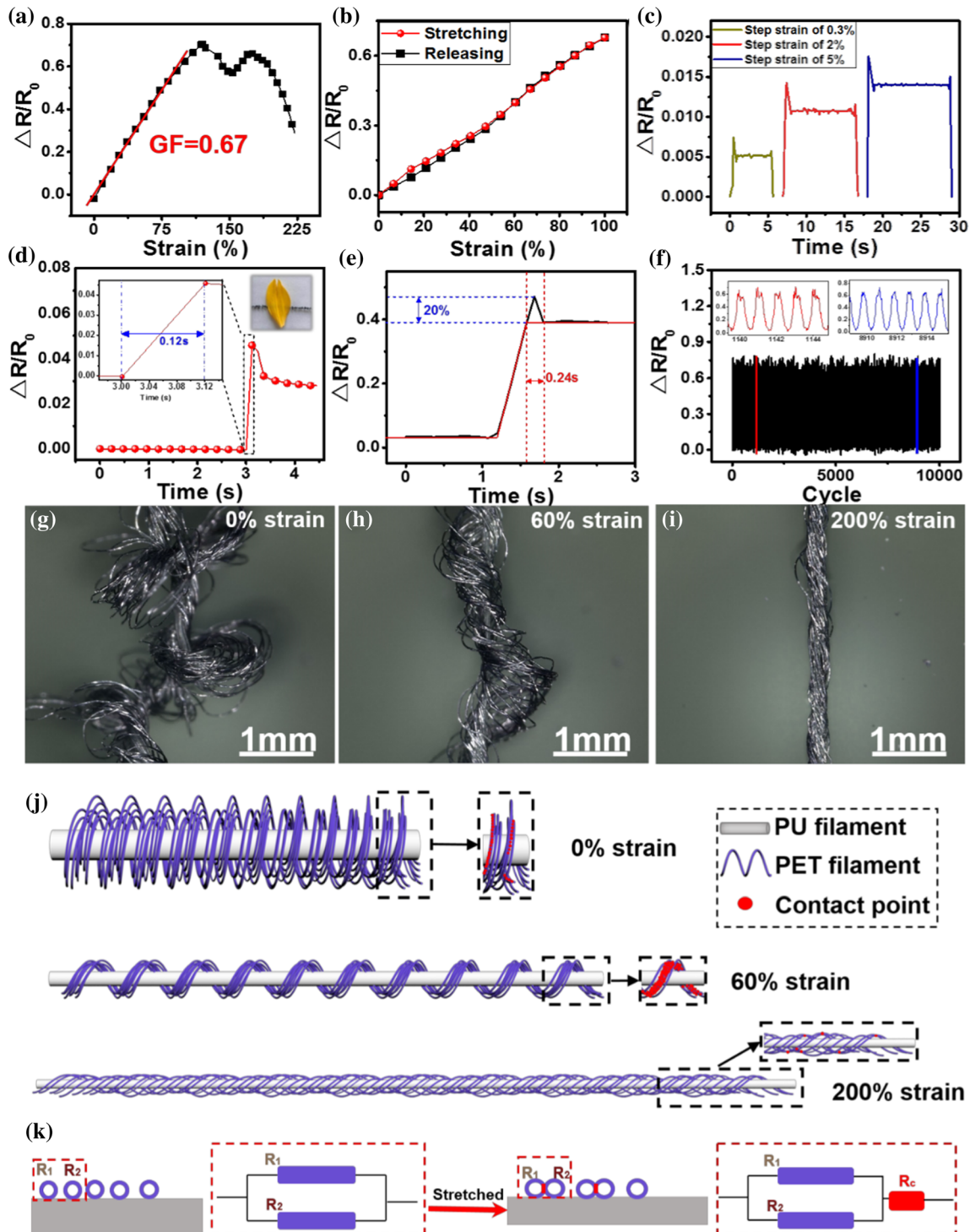
Figure 3 **a** Relative resistance variation of MCSY from 0 strain to 225% strain. **b** Relative resistance variation of GCSY under a 100% strain stretching–releasing cycle (strain rate of 30%/s). **c** Detection limit of the sensor under increasing step strain from 0.3 to 5% strain. **d** Response time of the GCSY. **e** Creep time of MCSY at a step strain of 20%. **f** Stability of a MCSY (5 cm) when stretched from 0 strain to 100% strain 10000 times (1HZ). **g–i** Photograph of MCSY at 0% strain and when it has been stretched to 60% strain and 200% strain. **j** Geometrical model of microstructure variation of GCSY and the GCSY before and after stretching. **k** The longitudinal section diagram of the MCSY before and after stretching.
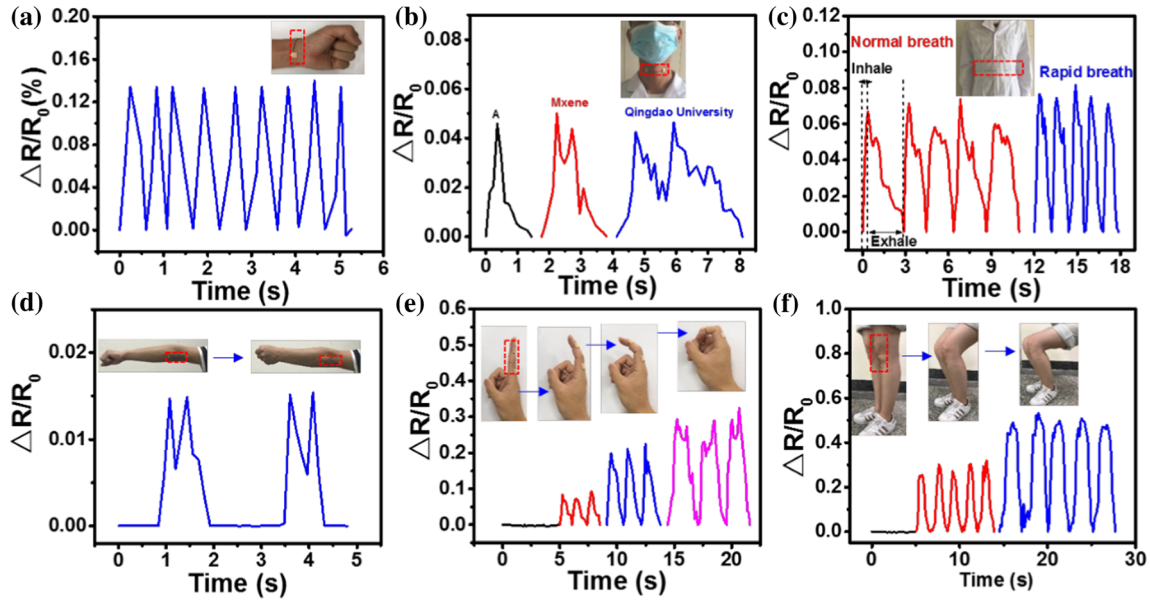
Figure 4 **a** Response curves of the wearer's wrist pulse. **b** Response curves of wearer spoke "A", "MXene" and "Qingdao University". **c** Response curves of the wearer's normal breath and rapid breath with the MCSY. **d** Response curves of twisting the forearm. **e**, **f** Response curves of bending finger and leg in different angles.

[18–21]. The introduced oxygen groups might enhance the hydrophilic properties of core-sheath yarns.

Strain and humidity-sensing properties of the MCSY

The sensing performance of MCSY is evaluated in Fig. 3. The resistance variation of MCSY under tensile strain ($\Delta R/R_0$) monotonically increases with tensile strain up to 120% (Fig. 3a). The relative resistance also has a good linearity with tensile strain up to 120%, and GF value is about 0.67. Figure 3b depicts the resistance variation of a 100% strain stretching–releasing cycle with margin hysteresis 23%. And the detection limit of MCSY could reach as small as 0.3% strain (Fig. 3c), and the response time is only 0.12 s by dropping a petal (Fig. 3d). MCSY also has a creep behavior, and the filament is revealing a percent overshoot (20%) and creep recovery time (0.24 s) (Fig. 3e). MCSY could also exhibit good durability, margin resistance variation even after 10000 times cycling (Fig. 3f). From the morphology of core-sheath yarns, the fluffy loops of PET sheath at the initial state (0% strain in Fig. 3g) are elongated and nearly cover PU core filament (120% strain in Fig. 3h). But the stretched PET loops are still at regularly loose loop structure. Once being stretched to 200% strain in

Fig. 3i, nearly all the PET filaments are tightly adhered on PU core surface, and PET filaments are mostly separated individually. Furthermore, the mechanism of resistance variation along with the stretching process is specified in Fig. 3j; during the stage of 0–120% strain, the number of contact points between PET filaments tends to more owing to the stretched loops structure. After 120% strain, from Fig. 3j, the number of contact point changes to less owing to the tightly loops structure. Here, we also established a longitudinal section diagram and resistance model to clarify the principle of resistance variation in Fig. 3k. The contact area among the PET filament and PET filament gradually increase during the stretching process, which lead to increase in the resistance of MCSY from 0 strain to 120% strain due to the generation of contact resistance.

To demonstrate potential applications of MCSY for the full-range detection of human activities, MCSY is employed to track human activities. As wearable yarn sensor, in terms of subtle deformation, the yarn sensor can identify the signal of the wrist pulse (Fig. 4a) and speaking (Fig. 4b). In terms of large deformation, the yarn sensor can identify the signal of forearm twisting (Fig. 4d), finger bending (Fig. 4e) and knee bending (Fig. 4f). Furthermore, our yarn-based sensor can be easily sewed, knitted or weaved
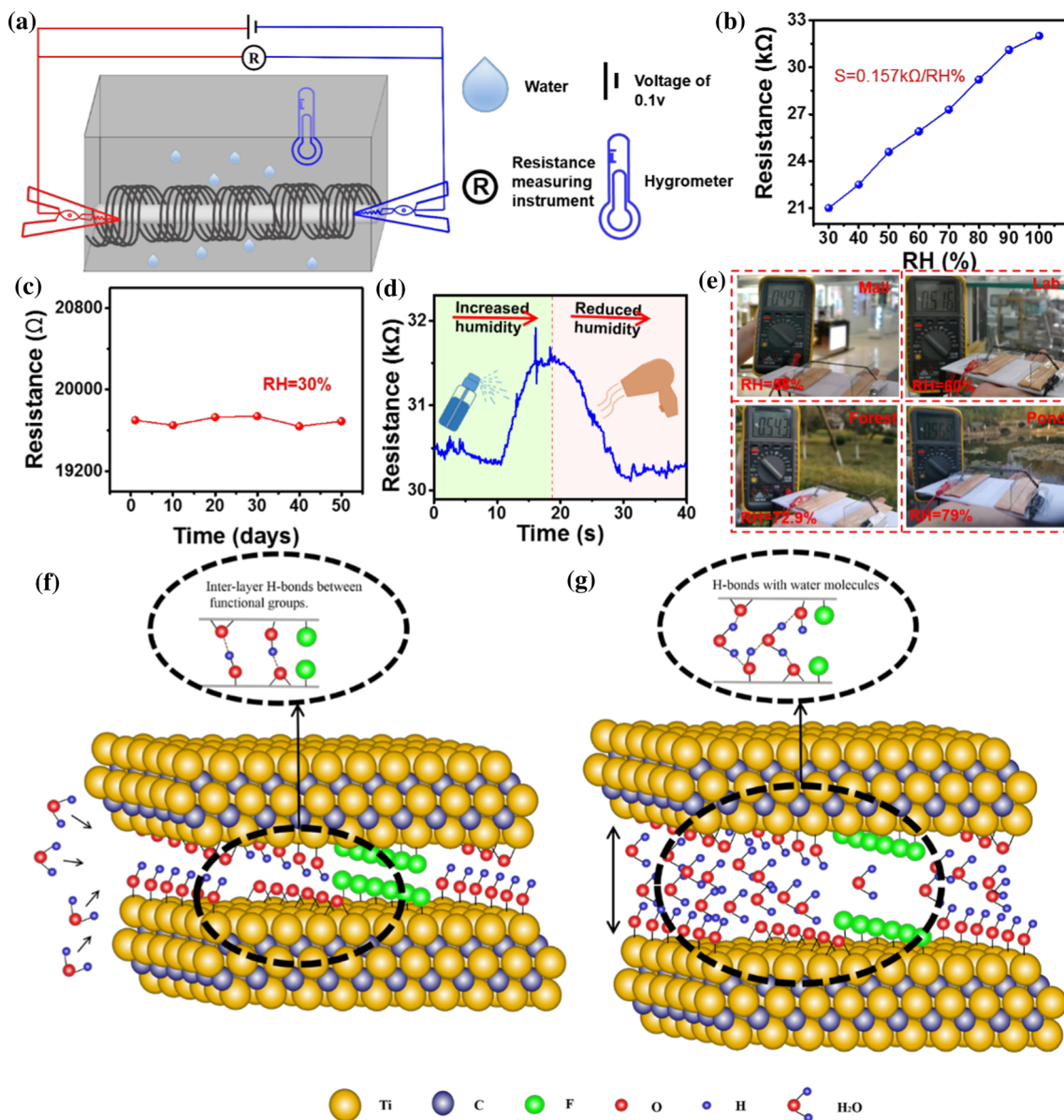
Figure 5 **a** Schematic illustration of the testing process of MCSY as a humidity sensor. **b** Resistance variation of MCSY from 40 to 100% humidity. (S = sensitivity) **c** Resistance variations with time for the MCSY samples at same RH levels. **d** Resistance variation of the yarn as it increases humidity and reduces humidity. **e** Resistance variation of MCSY in different environments. **f** Atomic structure of multilayer MXene. **g** Atomic structure of hydrated multilayer MXene.

into clothes with seamless integration and remarkable comfortable.

MCSY can also be utilized as a humidity sensor with good sensitivity. Figure 5a shows the schematic illustration of the testing process of MCSY as a humidity sensor resistance curve versus humidity is illustrated in Fig. 5b; the resistance of MCSY sample tended to linearly relationship with RH for approximately on a semi-logarithmic scale over the range of 30–100% RH, showing very high sensitivity and good

linearity. Furthermore, the humidity sensors exhibit stable performance even located in RH 30% conditions for 50 days (Fig. 5c). As shown in Fig. 5d, the resistive variations of MCSY can be immediately increased with the moisture exposed from the humidifier and then gradually dropped with the aid of heating blower. On the proof of concept, our humidity-sensing device was set at different scenarios (i.e., shopping mall, laboratory, forest and riverside), our device exhibited obviously different

resistivity, and the resistance at riverside responded the biggest value implying the highest humidity. Based on the FTIR spectra in Fig. 2c, some oxygen groups (epoxy and hydroxyl functional groups) introduced by MXene nanosheets could capture or release water molecules with the aid of H bonds as shown in Fig. 5f and g. MXene typically displays various configurations of the O·H bonds and inter-layer H-bonds between functional groups, as shown in Fig. 5f. With the incorporation of water molecules (Fig. 5g), the new hydrogen bond (H-bond) network between the inter-layer water molecules and the functional groups is established on individual MXene platelets. So, the distance between Ti_2C_3 layer from MXene tends to bigger after the water molecules connected with MXene intra-layer and inter-layer by a single H-bond (Fig. 5g). The bigger distance results in increase in the resistance of MCSY when the RH became higher [22].

Conclusions

In summary, we designed the wearable sensors with specific helical core-sheath structure that can detect most of human motions and humidity variation. At the same time, it has potential applications in daily life because of the diverse raw materials in textile field and its flexibility. The textile-based wearable sensors can achieve the seamless integration of clothing and sensors, which means that the clothes we wear in future can monitor motions or humidity directly.

Acknowledgements

Compliance with ethical standards

Conflict of interest No conflict of interest exits in the submission of this manuscript, and the manuscript has been viewed and approved by the authors.

References

[1] Liu MM, Pu X, Jiang CY et al (2017) Large-area all-textile pressure sensors for monitoring human motion and physiological signals. Adv Mater 29:3700–3708. https://doi.org/10.1002/adma.201703700

[2] Li Z, Tian M, Sun X, Zhao H, Zhu S, Zhang X (2019) Flexible all-solid planar fibrous cellulose nonwoven fabric-based supercapacitor via capillarity-assisted graphene/MnO^2 assembly. J Alloys Compd 782:986–994

[3] Miao JL, Chen S, Liu HH, Zhang XX (2018) Low-temperature nanowelding ultrathin silver nanowire sandwiched between polydopamine-functionalized graphene and conjugated polymer for highly stable and flexible transparent electrodes. Chem Eng J 345:260–270. https://doi.org/10.1016/j.cej.2018.03.144

[4] Sun FQ, Tian MW, Sun XT et al (2019) Stretchable conductive fibers of ultrahigh tensile strain and stable conductance enabled by a worm-shaped graphene microlayer. Nano Lett 19:6592–6599. https://doi.org/10.1021/acs.nanolett.9b02862

[5] Zhu Y, Shin B, Liu G, Shan F (2019) Electrospun ZnSnO nanofibers for neuromorphic transistors with ultralow energy consumption. IEEE Electron Device Lett 40:1776–1779. https://doi.org/10.1109/led.2019.2942342

[6] Zhang YZ, Lee KH, Anjum DH et al (2018) MXenes stretch hydrogel sensor performance to new limits. Sci Adv 4:eaat0098. https://doi.org/10.1126/sciadv.aat0098

[7] Cai GM, Yang MY, Xu ZL, Liu JG, Tang B, Wang XG (2017) Flexible and wearable strain sensing fabrics. Chem Eng J 325:396–403. https://doi.org/10.1016/j.cej.2017.05.091

[8] Hu X, Tian M, Xu T et al (2019) Multiscale disordered porous fibers for self-sensing and self-cooling integrated smart sportswear. ACS Nano 14:559–567. https://doi.org/10.1021/acsnano.9b06899

[9] Chen W, Huang G, Li X et al (2019) Revealing the position effect of an alkylthio side chain in phenyl-substituted benzodithiophene-based donor polymers on the photovoltaic performance of non-fullerene organic solar cells. ACS Appl Mater Interfaces 11:33173–33178. https://doi.org/10.1021/acsami.9b07112

[10] Cheng Y, Wang RR, Sun J, Gao L (2015) A stretchable and highly sensitive graphene-based fiber for sensing tensile strain, bending, and torsion. Adv Mater 27:7365–7371. https://doi.org/10.1002/adma.201503558

[11] Dinh T, Phan HP, Nguyen TK et al (2016) Environment-friendly carbon nanotube based flexible electronics for noninvasive and wearable healthcare. J Mater Chem C 4:10061–10068. https://doi.org/10.1039/c6tc02708c

[12] Kim I, Woo K, Zhong Z et al (2018) A photonic sintering derived Ag flake/nanoparticle-based highly sensitive stretchable strain sensor for human motion monitoring. Nanoscale 10:7890–7897. https://doi.org/10.1039/c7nr09421c

[13] Ma YN, Liu NS, Li LY et al (2017) A highly flexible and sensitive piezoresistive sensor based on MXene with greatly changed interlayer distances. Nat Commun 8:1207–1208. https://doi.org/10.1038/s41467-017-01136-9

[14] Kota S, Halim J, Lukatskaya M et al (2016) Synthesis and characterization of 2D molybdenum carbide (MXene). Adv Funct Mater 26:3118–3127. https://doi.org/10.1002/adfm.201505328

[15] An H, Habib T, Shah S et al (2018) Surface-agnostic highly stretchable and bendable conductive MXene multilayers. Sci Adv 4:eaaq0118. https://doi.org/10.1126/sciadv.aaq0118

[16] Muckley ES, Naguib M, Ivanov IN (2018) Multi-modal, ultrasensitive, wide-range humidity sensing with Ti_3C_2 film. Nanoscale 10:21689–21695. https://doi.org/10.1039/c8nr05170d

[17] Romer FM, Wiedwald U, Strusch T et al (2017) Controlling the conductivity of Ti_3C_2 MXenes by inductively coupled oxygen and hydrogen plasma treatment and humidity. RSC Adv 7:13097–13103. https://doi.org/10.1039/c6ra27505b

[18] Li LL, Frey M, Browning KJ (2010) Biodegradability study on cotton and polyester fabrics. J Eng Fiber Fabr 5:42–53. https://doi.org/10.1177/155892501000500406

[19] Jiao LL, Xiao HH, Wang QS, Sun JH (2013) Thermal degradation characteristics of rigid polyurethane foam and the volatile products analysis with TG-FTIR-MS. Polym Degrad Stab 98:2687–2696. https://doi.org/10.1016/j.polymdegradstab.2013.09.032

[20] Liu GZ, Shen J, Liu Q et al (2018) Ultrathin two-dimensional MXene membrane for pervaporation desalination. J Membr Sci 548:548–558. https://doi.org/10.1016/j.memsci.2017.11.065

[21] Xue Q, Zhang HJ, Zhu MS et al (2017) Photoluminescent Ti_3C_2 MXene quantum dots for multicolor cellular imaging. Adv Mater 29:4847–4852. https://doi.org/10.1002/adma.201604847

[22] Medhekar NV, Ramasubramaniam A, Ruoff RS, Shenoy VB (2010) Hydrogen bond networks in graphene oxide composite paper: structure and mechanical properties. ACS Nano 4:230–2306. https://doi.org/10.1021/nn901934u